ADVANCED MATERIALS INTERFACES
Open Access
www.advmatinterfaces.de

Facile Fabrication of Antibacterial 3D Fibrous Sponge via In Situ Protonation-Induced Direct Electrospinning

Altangerel Amarjargal, Olga Miler, Viraj P. Nirwan, Rebecca Hengsbach, Pawel Sajkiewicz, and Amir Fahmi**

A versatile, straightforward approach for direct fabrication of three-dimensional (3D) nanofibrous sponges via electrospinning is reported. The fabrication of porous 3D nanofibrous sponges is facilitated due to the protonation of dimethylamino ethyl (DMAE) groups in Eudragit E100 (EE). The generated 3D sponges are characterized by microscopy, thermal analysis, light scattering, and contact angle measurements to reveal their physicochemical properties. Additionally, antibacterial properties are confirmed via a colony-forming unit assay. Microscopy analysis demonstrated that the obtained nanofibers possessed uniform conformation without beads, and their overall diameter varies depending on the fraction of the blend composition. The protonation of DMAE groups is investigated via infrared spectroscopy and further confirmed via zeta potential measurements. The charged electrospun 3D sponges exhibited significant antibacterial properties, effectively combating *E. coli* even at a diluted extract of samples. Owing to their morphology, electrostatically charged surface, and significant antibacterial properties, these 3D nanofibrous sponges present themselves as an effective material for integration in filtering membranes or cartridges, which may minimize harmful substances suspended in the air.

1. Introduction

Polymeric blends represent a versatile category of composites where two or more polymers are combined via chemical or physical interactions to obtain a material with tailored properties.[1,2] Recent progress in the fabrication of nanomaterials has opened up exciting possibilities for creating advanced multifunctional composites with one, two, or three dimensions (1D, 2D, or 3D).[3,4] Among the diverse range of nanofabrication techniques, electrospinning stands out for its capacity to produce distinct structured electrospun membranes based on 1D nanofibers from polymer or polymer blended solutions in a cost-effective and reproducible manner.[5,6] Furthermore, it allows the combination of a wide array of incompatible materials, offering novel combinations with enhanced collective properties. The nonwoven structure of the resulting fibers boasts high porosity, interconnected pores, a high surface area-to-volume ratio, and a high strength-to-weight ratio.[7] Consequently, the tightly packed nanofiber layers provide smaller membrane thickness with pores, which is often advantageous in applications that require 2D sheet-like macrostructures. For instance, batteries equipped with thin yet mechanically robust separators produced by electrospinning have been shown to exhibit lower internal resistance, higher energy, and power densities.[8,9] Additionally, the pore sizes of resulting separators are sufficiently small to block the percolation of detached electrode particles and the formation of lithium dendrites. It has been observed that separators thinner than 25 µm possessing pores smaller than 1 µm are highly advantageous for such applications.[10]

On the other hand, applications such as air filtration, sound absorption,[11] and thermal insulation[12] favor fluffy 3D fibrous nanomaterials with controllable structure, lower density, and increased cavities. Here, an increase in surface area with very low density plays an essential role in the efficient filtering of particulate matter (dust particles or aerosols), which are often carriers of microbes and other hazardous substances.[13–15] Furthermore, it reduces the rate of pressure drop across the membrane over its lifecycle as compared to conventional 2D membranes.[16] The advantage of possessing the 3D structure in the case of tissue engineering scaffolds is well established. 3D nanofibrous scaffolds mimicking the natural extracellular matrix have been shown to promote cell proliferation and differentiation both in vitro and in vivo.[17–19] Therefore, a lot of resources have been devoted to

A. Amarjargal, V. P. Nirwan, R. Hengsbach, A. Fahmi
Faculty of Technology and Bionics
Rhine-Waal University of Applied Science
Marie-Curie-Straße 1, 47533 Kleve, Germany
E-mail: amarjargal.altangerel@hochschule-rhein-waal.de, amaraa1@must.edu.mn; Amir.Fahmi@hochschule-rhein-waal.de
A. Amarjargal
Power Engineering School
Mongolian University of Science and Technology
8th khoroo, Baga toiruu, Sukhbaatar district, Ulaanbaatar 14191, Mongolia
O. Miler, P. Sajkiewicz
Institute of Fundamental Technological Research
Polish Academy of Sciences
Pawińskiego 5b, Warsaw 02–106, Poland

The ORCID identification number(s) for the author(s) of this article can be found under https://doi.org/10.1002/admi.202400935

DOI: 10.1002/admi.202400935

the advancement of electrospinning technology, promoting efficient production of 3D nanofibrous materials. Largely, the fabrication strategies to obtain such a structure involve (a) the post-processing of conventional 2D non-woven mats or (b) the direct gathering of 3D nanofibers.[20,21] While the post-processing approach to change the non-woven mat into a 3D macroporous structure offers several benefits, such as a straightforward principle, excellent formability, and adjustable structure,[22–24] there are still some concerns with the conversion process. Since it includes time-consuming steps such as a gas production process or a chopping dispersion of the nanofiber mesh in an aqueous solution followed by freeze-drying.[25–27] Moreover, there are accompanying risks, such as potential toxicity from foaming agents and the loss of bioactive compounds encapsulated in nanofibers.[28] The direct preparation method for 3D fibrous materials with a fluffy texture, which involves manipulating the working parameters of electrospinning, inherently overcomes the drawbacks associated with post-processing conventional 2D meshes. However, many of these methods necessitate an extra high-voltage generator,[29] a spinning chamber with controlled humidity,[30,31] a special template/collector system,[32–35] or the addition of toxic components to the spinning solution to tune crucial parameters.[36–39]

This study aims to fabricate an antibacterial 3D nanofibrous sponge through conventional electrospinning using a selection of solvents, avoiding potentially toxic additives or additional steps. Eudragit E100 (EE), a non-toxic cationic polyelectrolyte[40] belonging to a class of polymethacrylate-based copolymers, was selected as the functional additive to prepare the blended spinning solution. Because of their abundant charged functional groups, polyelectrolytes and some organic acids are known to cause considerable repulsion in spinning jets, which facilitates the creation of electrospun 3D structures.[33,41] Here, the hypothesis was that blending of EE with an acidic polymer solution would not only be crucial in the fabrication process, serving as a source of in situ protonated dimethylaminoethyl (DMAE) groups to promote like-charge repulsions but at the same time, the introduced charges will also impart antibacterial properties to the fabricated 3D structure.[5] To the best of our knowledge, this is the first existing report on a one-step method that introduces three-dimensionality and an antimicrobial effect to nanofibrous matrices through in situ protonation of the polymer blend. Significantly, the simplicity and versatility of the proposed method allows the fabrication of electrospun nanofibers into 3D sponge-like macrostructures from various combinations of polymers such as cellulose acetate (CA), polymethylmethacrylate (PMMA), polycaprolactone (PCL), and gelatin (Gel). Essentially, creating a platform for further development and functionalization for a broad range of potential applications.

2. Experimental Section

2.1. Materials

Cellulose acetate (CA, Mw = 100 000 g mol^{-1}) was purchased from Thermo Scientific. Polymethylmethacrylate (PMMA, Mw = 100 000 g mol^{-1}) was purchased from Polyscience. Gelatin (Gel, type B with Bloom ≈225 g) and polycaprolactone (PCL, Mn = 80 000 g mol^{-1}) were purchased from Sigma–Aldrich. A copolymer of methyl methacrylate, dimethyl aminoethyl methacrylate, and butyl methacrylate, Eudragit E 100 (EE, Mw = 47000 g mol^{-1}), was provided by Evonik GmbH (Darmstadt, Germany). N, N-dimethylformamide (DMF, 99.8%), acetone (Ac, 99.8%), trifluoroacetic acid (TFA, 99,9%), formic acid (FA, 95%), and chloroform (CHL, 99%) were obtained from Carl Roth. Lysogeny broth (LB) and lysogeny broth agar (LB agar) were purchased from A&A Biotechnology (Gdansk, Poland). Bacteriological agar was purchased from Merck Life Science (Poznan, Poland). Gram-negative bacterium *E. coli* DH5α was obtained from the Laboratory of Calcium Binding Protein, Nencki Institute of Experimental Biology PAS (Warsaw, Poland), and gram-positive bacterium *S. aureus* ATCC 6538 was purchased from Argenta (Poznan, Poland).

2.2. Preparation of 2D Membrane and 3D Sponges by Blend Electrospinning

Two distinct solutions (based on EE and support polymer, separately) were intended for blend electrospinning. EE solution was prepared in CHL, while different support polymer solutions (CA, Gel, PCL, PMMA) were prepared separately by dissolving appropriate amounts in an acidic solvent (TFA and FA). Following preliminary experiments that explored how different ratios affect the structural integrity of the 3D architecture, appropriate amounts of solutions were blended to achieve a 3:2 weight percentage ratio of support polymer to EE. The blend solution was stirred (200 rpm) for 2–4 h at room temperature. For comparison, another CA/EE solution was prepared using the same methodology using non-acidic solvents (Ac for support polymer and DMF for EE). Then, the spinning solution was loaded into a 5 mL syringe ended with a 21G needle. Electrospinning was performed with the nozzle fixed in a vertical position at room temperature and humidity (22–25 °C and 30%–45%, respectively). The resulting nanofibers were gathered on a flat collector. **Table 1** provides details of the sample names, solvents used to dissolve the polymers, the solution's electrical conductivity, and electrospinning parameters.

2.3. Characterization

2.3.1. Electrical Conductivity Measurements of the Spinning Solutions

The electrical conductivities of the spinning solutions were measured in triplicate at room temperature with a conductivity meter (Greisinger G1409-L01, Germany). The measured values of solution conductivity are shown in Table 1.

2.3.2. Scanning Electron Microscopy (SEM)

The morphology of 2D and 3D nanofibrous samples was revealed using SEM (JEOL JSM-IT100; Japan/Zeiss, Germany). Before SEM imaging, the samples were affixed to aluminum stubs using carbon tape and coated with a thin layer of gold for 60 s with a Crossington Sputter Coater 108 Auto, enhancing the signal-to-noise ratio. The observations were done at the acceleration of the

Table 1. Details of the nanofibrous membrane and sponge materials: composition of the solutions, electrical conductivity, and parameters of the electrospinning process.

Sample name	Polymer concentration [%, w/w]		Solvent	Conductivity [mS cm^{-1}]	Flow rate [mLh^{-1}]	Tip-to-collector distance [cm]	High voltage [kV]
2D CA/EE	CA	15	Ac	0.047 ± 0.01	0.3	15	20
	EE	40	DMF				
3D CA/EE	CA	16	TFA	0.73 ± 0.06	0.4	30	18
	EE	30	CHL				
3D Gel/EE	Gel	25	FA	4.71 ± 0.03	0.3	30	16
	EE	30	CHL				
3D PCL/EE	PCL	20	FA	1.37 ± 0.05	0.3	30	16
	EE	30	CHL				
3D PMMA/EE	PMMA	25	TFA	0.10 ± 0.02	0.4	30	18
	EE	30	CHL				

applied voltage, ranging from 15 to 18 kV. Selected magnifications were documented. The fiber diameter distributions were calculated by means of 100 measurements performed on random locations of the materials using the ImageJ software. The diameter distributions were presented in histograms.

2.3.3. Porosity Measurements

The porosity of the samples was evaluated using the liquid pycnometer technique.[29] Cyclohexane was selected as the liquid displacement due to its ability to penetrate through samples without dissolving the fibers. Initially, the weight of the pycnometer filled with cyclohexane was recorded as W_1. Subsequently, dry samples W_s were immersed, and air bubbles were removed under vacuum to allow cyclohexane to fill the pores. The pycnometer was then filled with cyclohexane again, and the whole weight was denoted as W_2. Finally, after removing the samples, the weight of the remaining cyclohexane and pycnometer was measured as W_3. The porosity of the 2D membrane and 3D sponges was then calculated according to the Equation (1):

$$Porosity\,(\%) = \frac{W_2 - W_3 - W_s}{W_2 - W_1} \quad (1)$$

2.3.4. Attenuated Total Reflectance (ATR)- Fourier Transform Infrared Spectroscopy (FTIR)

The analysis of chemical groups present within the components of the nanofibers was conducted using the PerkinElmer Frontier spectrometer with an ATR assembly. The ATR-FTIR spectra of the 2D and 3D materials were captured within the range of 600–4000 cm^{-1}. The spectral resolution was 2 cm^{-1} with an accuracy of ±1 cm^{-1}.

2.3.5. Thermogravimetric Analysis (TGA)

The thermal stability of the materials was assessed using a thermogravimetric analyzer (TGA 4000, PerkinElmer). Fibrous samples of 10 mg were placed in a ceramic cuvette, and heated at a rate of 10 °C min^{-1}, starting from 35 °C and reaching 700 °C. All measurements were conducted under nitrogen flow with a flow rate of 20 mL min^{-1}.

2.3.6. Zeta Potential Measurements

Zeta potential measurements were done at Malvern Zetasizer NanoS by Malvern Instruments equipped with a HeNe laser (λ = 633 nm) with P = 4 mW. 10 mg of sample were crushed with a pestle in an agate mortar. Subsequently, they were dispersed in 10 mL ethanol through ultrasonication. Measurements were done at 25 °C after equilibrating for 120. Three measurements were made for each sample, with 15 repetitions for each measurement. DTS1070 cuvettes were used.

2.3.7. Contact Angle Measurements

The surface wettability of the samples, expressed by the contact angle, was measured with a goniometer using a sessile drop method (Data Physics OCA 15EC, Filderstadt, Germany). The angle was measured immediately after placing the droplet on the material and after 5, 10, 30, 60, and 90 s, using freeze frames from recorded videos. For each material, 5 separate measurements were done.

2.4. Antibacterial Assessments

2.4.1. Bacterial Culture

E. coli (DH5α) and *S. aureus* (ATCC 6538) were cultured on LB agar and isolated with a streak plate method. Before the test, an isolated colony was inoculated in 3 mL of fresh LB and left overnight to grow in an orbital shaker at 37 °C.

2.4.2. Antimicrobial Activity Suspension Test

Materials were cut into samples of equal mass (15 mg) and sterilized under UV light for 1 h on both sides (30 min per sample

side) to reduce the bioburden. Then, they were put for 24 h in 5 mL tubes filled with 2 mL of sterile LB and kept in an incubator (37 °C) for 24 h. Extracts obtained this way were filtered through 0.2 µm syringe filters to remove larger parts of materials suspended in the medium, which could alter the results. Each extract was diluted with LB to the following concentrations: 50%, 25%, 12.5%, and 6.25%, to be tested together with the stock.

Right before the test, the concentration of the overnight bacterial cultures of *E. coli* and *S. aureus* in LB was adjusted with fresh LB to $\approx 10^6$ colony-forming units (CFU) mL^{-1}. In 96-well plates, 100 µL of bacterial suspension and 100 µL of extracts and their dilutions (or pure LB for positive controls) were incubated together for 2 h. After this time, the suspensions were serially diluted with PBS in another 96-well plates, and each dilution was plated on LB agar in three technical repetitions. After overnight incubation at 37 °C, bacterial colonies were counted to estimate cell survival after contact with the materials. Additionally, 100 µL of each undiluted suspension of inoculated extracts of 100%, 50%, 25%, and 6.25% were evenly spread on separate LB agar plates with sterile spreaders, and the plates were incubated at 37 °C overnight. The test was conducted in triplicate.

3. Results and Discussion

3.1. Fabrication of Electrospun 2D Membrane and 3D Sponges

It is widely accepted that adjusting the composition of the spinning solution can affect the spatial arrangement of the nanofibers on the surface of the collector and may result in the formation of 3D structured materials.[38,39] In the present study, we proposed a straightforward fabrication of a 3D nanofibrous sponge by direct electrospinning of an in situ protonated pH-responsive polyelectrolyte blend solution. Earlier studies have shown that electrospinning of polyelectrolytes with high charge density, where the charges are located on the surface or close to it, facilitates the formation of complex 3D configurations.[41,42] For polyelectrolytes like sodium alginate, 3D nanofibrous structures can be fabricated by offsetting their insufficient charge density through controlled humidity and the use of surfactants. The presence of high humidity leads to the dissociation of the polyelectrolyte into charged groups ($R\text{-}COO^-$, Na^+), thereby increasing its charge density.[41] The technique presented here allows for increasing the charge density of polyelectrolytes, which is vital in forming fluffy nanofibrous macrostructures. Resulting in an easy and accessible strategy that does not require controlled humidity while spinning or the addition of toxic surfactants in the electrospinning solution. The underlying hypothesis was that EE could be an effective functional additive for preparing protonated polymer blends from an acidic solvent system, thereby increasing charge density. This hypothesis was corroborated by the significantly higher electrical conductivity measured in the CA/EE blend when prepared in TFA/CHL (0.73 ± 0.01 mS cm^{-1}), compared to the CA/EE blend in Ac/DMF (0.047 ± 0.01 mS cm^{-1}). The increased conductivity can be attributed directly to the in situ protonation of the DMAE groups.

The microscopic morphology and diameter distribution of fibers from the samples are depicted in **Figure 1**. As observed from the optical images and SEM micrographs (Figure 1a,b), CA/EE dissolved in Ac/DMF solvent was electrospun into a conventional 2D sheet-like fibrous membrane featuring randomly oriented nanofibers, and diameter distribution was determined to be 324 ± 198 nm. Upon changing the solvent system to acidic TFA/CHL, a significant change was observed in the deposition of nanofibers during electrospinning. As the high voltage was applied, the nanofibers actively aligned themselves toward the collector within a minute, creating a robust nanofiber stack standing perpendicular to the collector's surface (Movie S1, Supporting Information). As the electrospinning continued, subsequent nanofibers were deposited on the top, leading to the formation of 3D sponge-like structures (CA/EE; Figure 1b inset and Movie S2, Supporting Information). The SEM micrograph shows that the 3D CA/EE sponge possesses sparsely distributed nanofibers with an average diameter of 343 ± 86 nm and demonstrated larger pore sizes than the control nanofiber membrane (2D CA/EE). (Figure 1c,d). To verify the versatility of the method, several polymers, including PCL, Gel, and PMMA, were combined with EE to obtain electrospun 3D sponges. As expected, all these polymers were successfully electrospun into fluffy 3D fibrous macrostructures (Figure 1e,g,i; Movie S3, Supporting Information). The average nanofiber diameters inside these sponges, as measured with ImageJ, were 873 ± 166 , 1134 ± 204 , and 2178 ± 642 nm for 3D Gel/EE, 3D PCL/EE, and 3D PMMA/EE, respectively (Figure 1f,h,j). Compared to the fabrication of 3D nanofibrous sponges that have been reported before,[33–35] the advantage of our strategy is that a conventional electrospinning setup can be used with some modifications, to the blended spinning solution, yielding nanofibers with uniform diameters as fluffy macrostructures.

By blending EE with support polymers dissolved in different solvents (acidic and non-acidic), distinct nanofibrous materials with different spatial dimensions, i.e., conventional 2D membranes and advanced 3D sponges, were electrospun. The variations in 2D and 3D electrospun structures result from the presence of non-protonated and protonated[41] DMAE groups in EE.[43] The non-acidic solvent system chosen for electrospun 2D membranes did not change the state of the DMAE groups. Due to the absence of charged amine groups, the repulsive forces between the nanofibers are lower, allowing the nanofiber layers to be deposited tightly on top of each other on the collector (**Figure 2a**). In contrast, when EE is blended with an acidic solution, protonation occurs, increasing the density of positively charged DMAE groups across the polymer chain. Through the electrospinning process, the distribution of such charged groups primarily occurs on or near the outer surface of nanofibers,[37,41] generating electrostatic repulsive forces between neighboring nanofibers, leading to porous 3D structures. It is important to highlight that our initial screening experiments demonstrated that the blend solution with a lower content of EE (at a ratio less than 4:1) failed to yield the desired fluffy nanofibrous macrostructure (Movie S4, Supporting Information). The observed outcome may be primarily attributed to the insufficient amount of charged DMAE groups throughout the polymer chain. This deficiency leads to insufficient charge repulsion between the as-spun fibers during the spinning process, which impacts the overall construction of the 3D sponge.

The distinctive fluffy architecture of 3D nanofibrous sponges has undergone extensive research due to its large porosity, ultralow bulk density, and flexibility. These characteristics are well

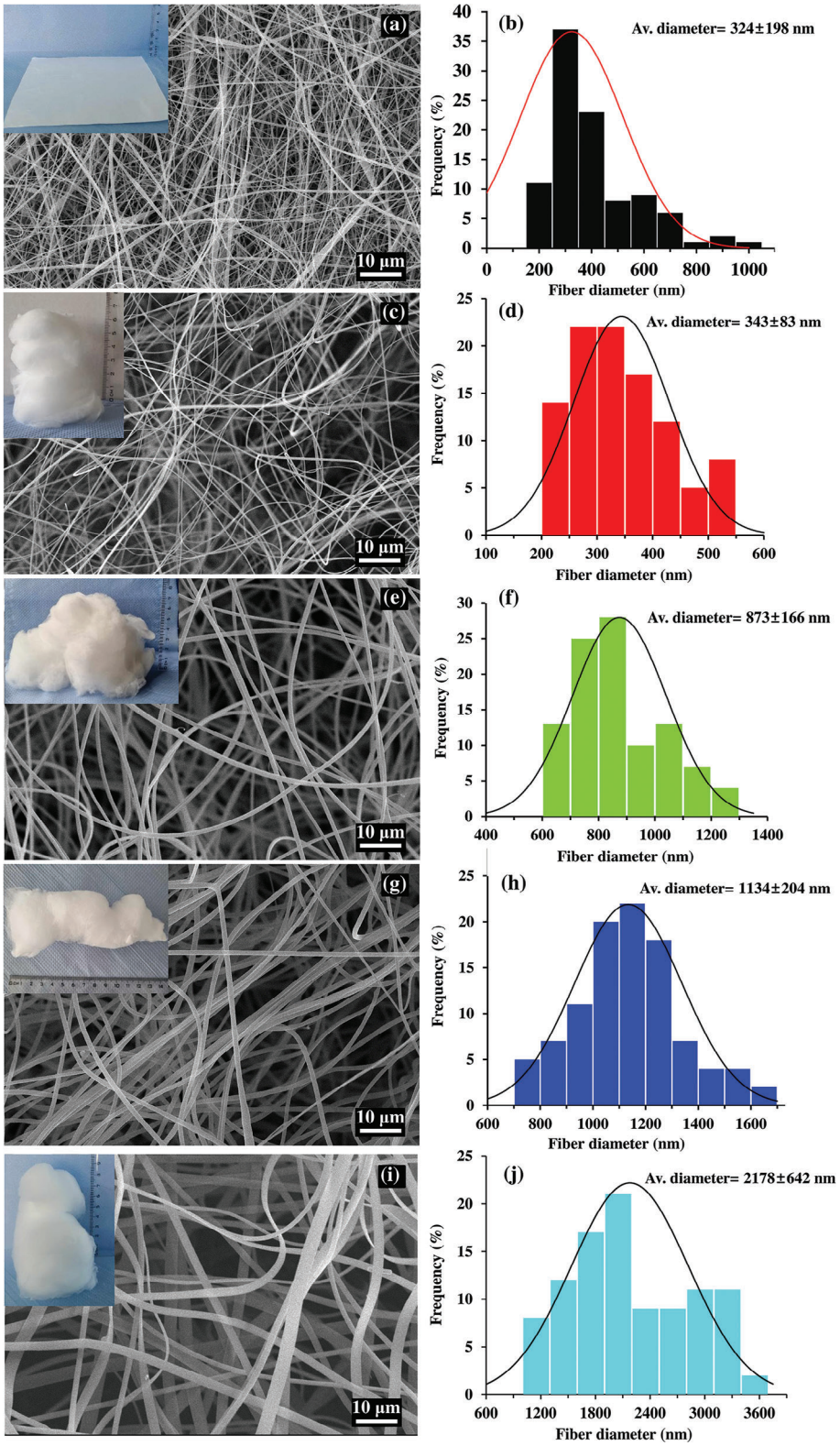

Figure 1. SEM micrographs and diameter distribution of the nanofibers originating from solutions of: CA/EE in DMF/Ac a,b) and TFA/CHL c,d), Gel/EE in FA/CHL e,f), PCL/EE in FA/CHL g,h), PMMA/EE in TFA/CHL i,j). Insets are optical images of each sample.

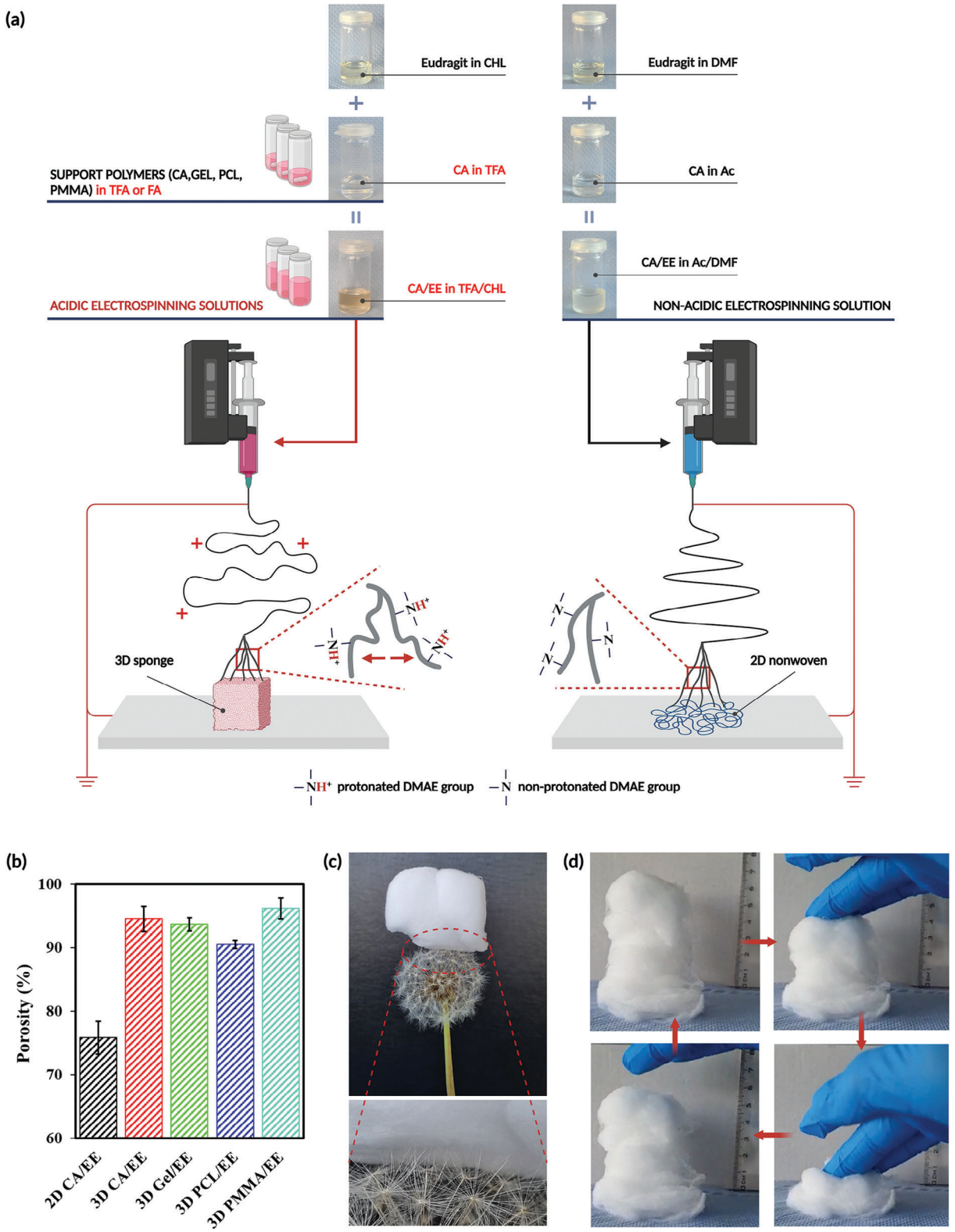

Figure 2. Illustration of in situ protonation-induced electrospinning of 3D structures for direct fabrication of various polymeric nanofibrous sponges compared to conventional electrospinning of a 2D membrane a) The porosity of 2D nanofiber membrane and 3D nanofiber sponges b). A piece of a 3D CA/EE sponge poised atop the hairs of a dandelion c). The sponge made of 3D CA/EE nanofibers can be effortlessly returned to its original state following various compression levels d). Figure drawn utilizing BioRender. Miler, O. (2025) https://BioRender.com/j97i455.

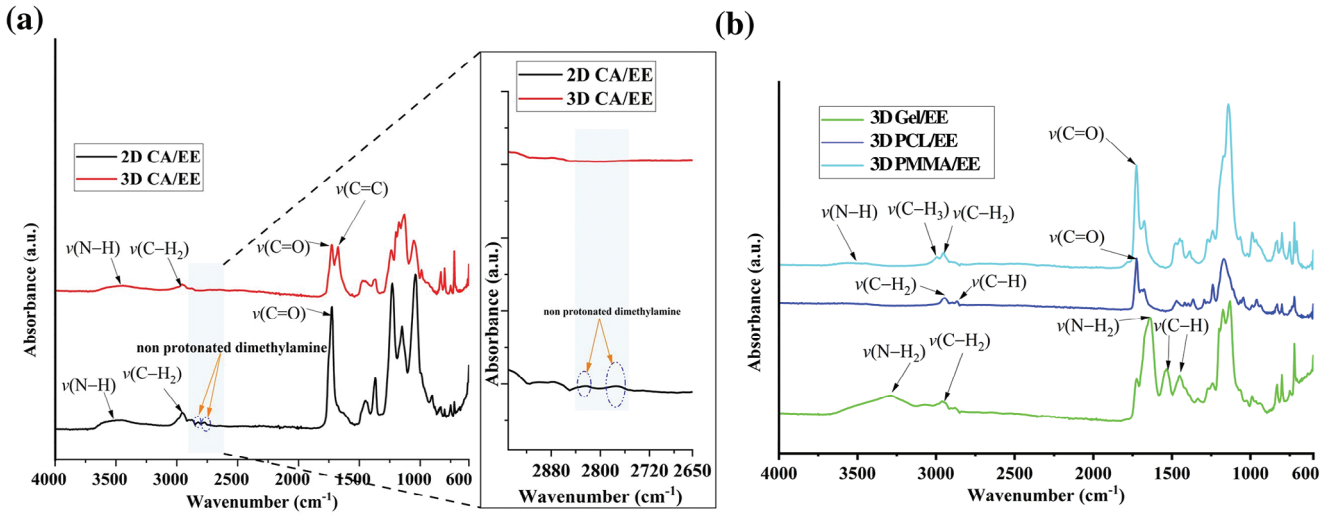

Figure 3. ATR-FTIR spectra of the electrospun materials: comparison of 2D CA/EE membrane and 3D CA/EE sponge with a close-up view on DMAE region a) and a compilation of spectra of 3D Gel/EE, 3D PCL/EE and 3D PMMA/EE materials b). Important regions and peaks are highlighted and labeled.

recognized for a wide range of potential applications.[11,12,19] Likewise, our 3D fibrous sponges exhibited more than 90% porosity (Figure 2b) and can be characterized as ultralight materials, as shown in the example of the 3D CA/EE sponge (Figure S1, Supporting Information), which could rest on the delicate hairs of a dandelion without causing deformation, as depicted in Figure 2c. Furthermore, due to robust structural integrity and excellent compressibility, the sponge readily regains shape after repeated compressive forces. (Figure 2d; Movie S5, Supporting Information).

3.2. Attenuated Total Reflectance- Fourier Transform Infrared Spectroscopy

The electrospinning of nanofibers into 3D structures presumably results from the protonated DMAE groups of the EE backbone, originating by the usage of acidic solvents. Hence, ATR-FTIR was used to analyze the interactions among the polymers used to fabricate nanofibers and confirm the presence of the protonated DMAE groups in the 3D sponges. As seen in **Figure** 3a, the 2D CA/EE and 3D CA/EE materials were scanned from 4000 to 600 cm^{-1}. Both samples show a broad secondary amine absorbance peak that is associated with EE in the samples at 3490 cm^{-1}. At 2947 cm^{-1}, a weak aldehyde C—H stretch could be observed due to the presence of cellulose acetate. Interestingly, two absorbance peaks at 2820 and 2770 cm^{-1} that are associated with the symmetric stretching of the non-protonated state of the DMAE group were absent in 3D CA/EE samples.[44,45] The absence of this peak in 3D CA/EE samples supports the hypothesis that the protonation of the DMAE group was the major contributing factor to the change in the packing density of nanofibers during deposition.[46] Eventually, leading to the fabrication of 3D nanofibers. A strong peak for C═O aldehyde stretch can be observed at 1720 cm^{-1}. In the 2D sample, the C═C stretch absorbance band was not observed as opposed to 3D samples, where it can be observed at 1672 cm^{-1}. Between 1453 and 1040 cm^{-1}, there are several overlapping absorbance peaks related to C—H bend, C—O, and C—N stretch that are visible in both 2D and 3D samples. O—H bend associated with carboxylic acids from cellulose acetate is, however, visible only in 2D membrane and is restricted in 3D sponge.

3D nanofibrous sponges containing EE blended with Gel, PCL, and PMMA were also analyzed by ATR-FTIR (Figure 3b). Here, it could be observed that the absorbance bands of 3D PCL/EE and 3D PMMA/EE sponges were almost superimposable with some change in absorbance intensities. One of the differences was the presence of a secondary amine absorbance peak that is associated with the EE from 3600 to 3366 cm^{-1} in 3D PMMA/EE.[6] Additionally, in 3D PCL/EE nanofiber sponge, an absorbance peak could be observed at 2868 cm^{-1} caused by C—H_2 asymmetric stretch corresponding to PCL.[47] Whereas 3D Gel/EE nanofiber sponge showed absorbance peaks at 3285 cm^{-1} due to the presence of several amine groups, aromatic C—H stretches at 3087 , 1546 , and 1449 cm^{-1}, and primary amine bend at 1632 cm^{-1}.[48,49] The absorbance behavior in the fingerprint region of spectra is more or less similar, and significant changes are not observed. Interestingly, the changes in the solution facilitating the formation of 3D structures are discerned clearly by ATR-FTIR. Moreover, functional groups identical to the polymers blended with EE could be resolved.

3.3. Thermogravimetric Analysis

The thermal degradation behavior and the corresponding mass loss of the electrospun 2D membrane and 3D sponges were measured using TGA. Moreover, the derivative thermogravimetric (DTG) graph revealed the individual weight loss events associated with the respective polymer of each type of nanofiber. The results are summarized in **Table** 2. As seen from the TGA graph in **Figure** 4a, all the nanofiber samples show a multi-step degradation profile. The onset temperature observed in the case of a 2D membrane is higher than that of a 3D CA/EE sponge. However,

Table 2. Results of TGA of the nanofibers depicting their main degradation events, namely the onset temperature (T_{Onset}), the Endpoint of mass loss ($T_{Endpoint}$), and the inflection point of graphs ($T_{Inflection\ point}$) as well as the total weight loss.

Sample name	T_{Onset} [°C]	$T_{Endpoint}$ [°C]	$T_{Inflection\ point}$ [°C]	Weight loss [%]
2D CA/EE	331	430	382	88
3D CA/EE	311	440	391	91.4
3D Gel/EE	223	373	257	84.2
3D PCL/EE	395	462	435	97.7
3D PMMA/EE	359	458	422	98.6

the inflection temperature and end temperature for 3D CA/EE are measured to be higher. Here, the total weight loss at the end of the temperature program was observed to be 3% higher in the case of 3D CA/EE nanofibers. The compactness of the 2D sample could be one reason for a lower weight loss and higher onset temperature. In the DTG curve, 2D and 3D CA/EE show a slight weight loss before 100 °C, which might be attributed to water loss. At 248 °C, a significant weight loss event is observed for 3D CA/EE, which coincides with a similar weight loss in 2D CA/EE, however, to a lower level. The weight loss at this temperature can be attributed to the first degradation event associated with EE. It can be observed in all the samples with varying magnitudes around the same temperature range.[50] The thermal degradation of CA in 2D CA/EE and 3D CA/EE was observed between 313 and 320 °C.[51] Another major weight loss event related to the complete degradation of nanofibers was observed at 382 and 390 °C for 2D CA/EE and 3D CA/EE, respectively. For both samples, the main mass loss occurred before 496 °C, and there was no further mass change afterward. The first thermal degradation of EE could be observed at 251, 242, and 243 °C for 3D Gel/EE, 3D PCL/EE, and 3D PMMA/EE, respectively. Interestingly, 3D Gel/EE showed the lowest onset temperature and lowest weight loss. These nanofibers contained the highest moisture among all the samples, which can be seen in Figure 4b due to the mass loss peak observed ≈79 °C. The major degradation associated with Gel in 3D Gel/EE takes place at 360 °C,[48] while another thermal degradation occurred at 456 °C. A partial degradation of 3D PCL/EE and 3D PMMA/EE was observed at 324 and 311 °C, respectively. Finally, the major weight loss events for 3D PCL/EE and 3D PMMA/EE nanofibers were measured at 438 and 427 °C, respectively.[6,52,53]

3.4. Zeta Potential Measurements

To further verify the protonation of DMAE in EE, zeta potential measurements were performed. However, as the zeta potential is obtained using electrophoretic mobility, it is not always well-described for polymeric structures.[54,55] For nanofibers, we need to consider the shape, more precisely, the high length-to-diameter ratio, which is far away from ideal spheres, considered standard for measurement. The measurements served primarily to confirm the more pronounced positive charges on the 3D nanofibrous sponges.

The zeta potential of the 2D CA/EE membrane was around +3 mV, significantly lower than the measured potentials of all 3D fibrous sponges, ranging from +38 to +55 mV, indicating the non-protonated DMAE groups of EE in the 2D structures and the protonated DMAE groups of EE in the 3D structures, respectively (**Figure 5**). With that, it can be concluded that an electrostatic repulsion within the protonated 3D nanofibrous sponges exists. During the electrospinning process, such electrostatic repulsion influences the structure significantly, leading to loosely packed fiber at the nanoscale as well as 3D structures seen macroscopically.[56,57]

3.5. Contact Angle Measurements

It has been reported that protonated groups in polymeric structures lead to enhanced hydrophilic properties accompanied by changes in the conformation of the polymer backbone.[58] Thus, water contact angle measurements for electrospun 2D membrane and 3D sponges were performed to investigate the sample's wettability properties (**Figure 6**). The measurements were performed on a flat surface, which, in the case of the 2D material, was a spread nonwoven fabric, and in the case of the 3D materials, was a scalpel-cut or originally flat fragment. Caused by the hydrophobicity of EE,[43,59] 2D CA/EE nanofibrous membrane is hydrophobic with almost constant contact angles of above 100° for the studied time period, even though the CA molecular chain

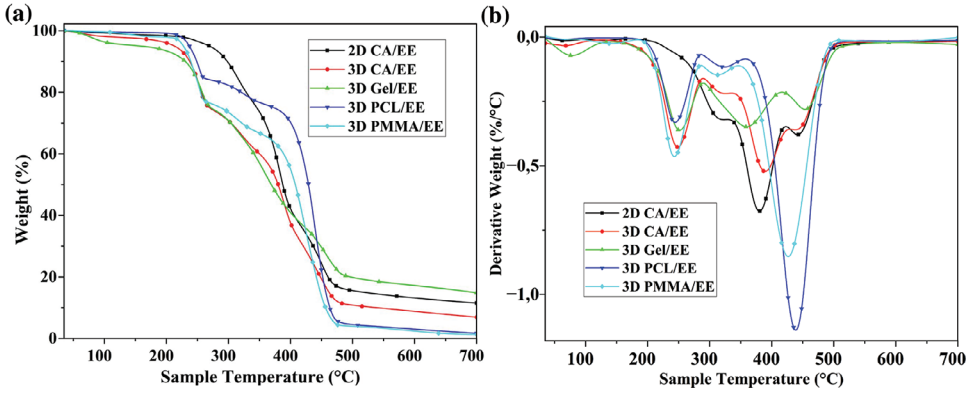

Figure 4. Results of TGA of the electrospun materials with mass loss during heating in comparison for different nanofiber compositions a) and the abrupt nature of mass loss shown in DTG graphs – each peak represents a major mass loss b).

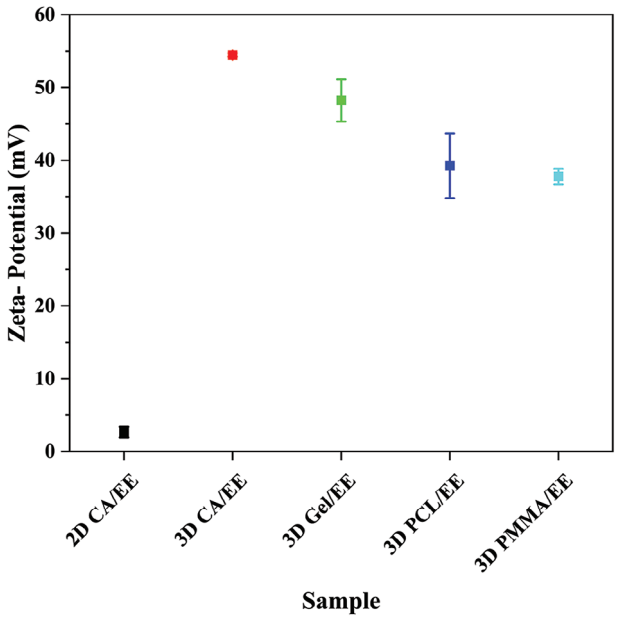

Figure 5. Zeta potentials of the nanofibers dispersed in ethanol. Three measurements with 15 repetitions were done for each sample to determine the mean value with standard deviation. Error bars are partially within the range of the symbols.

contains hydrophilic OH groups.[60] The contact angle only decreased slightly over time, possibly due to the capillary forces of most of the nonwoven exterior layer, which consisted of loose bunches of fibers.

In contrast, 3D CA/EE was found to be highly hydrophilic, absorbing water droplets within a maximum of 90 s. Since the cellulose OH groups were not visible in the ATR-FTIR spectrum (Figure 3), it might be concluded that DMAE groups in EE have been effectively protonated and are located on the exterior part of the fibers, leading to increased hydrophilicity. 3D Gel/EE and 3D PCL/EE sponges exhibited similar characteristics, with 3D Gel/EE absorbing water the quickest. While the hydrophilicity of 3D Gel/EE nanofibrous sponge might have resulted from the hydrophilicity of Gel, the hydrophilic nature of 3D PCL/EE could only be explained by the protonation of DMAE.[61,62] The 3D PMMA/EE sample initially exhibited hydrophobic characteristics, effectively repelling water for the first 90 s of observation. However, as the measurement period extended, the sample began to show hydrophilic behavior (data not shown). On all 3D samples, the initial contact angles of the droplets were higher than those of 2D CA/EE material. It could also be observed through the goniometer lens that the contact angle on 3D materials initially changed mostly due to capillary forces soaking water into the pores, most probably reflecting the Cassie-Baxter to Wenzel state transformation. Thus, initial angle measurements represented apparent contact angles.[63]

The wettability of a material is considered to be an important parameter for the effective interaction with biological matter. It allows a high area of contact, enhanced surface activity, and adhesion of cellular proteins. Materials with higher hydrophobicity reduce cell adhesion, which might, unfavorably, hinder the accessibility of antibacterial chemical groups to the cytoplasmic membrane of bacteria.[64]

3.6. Antibacterial Study

As discussed in the introduction section, the primary objective of this research was to develop and validate the effectiveness of an antibacterial 3D nanofibrous sponge. The tests were performed on gram-negative (*E. coli*) and gram-positive (*S. aureus*) model bacterial strains (**Figure 7**). After just 2 h of incubation, the material extracts of all 3D samples reduced the concentration of *E. coli* by more than 4 log, below the detection limit (>99,99% CFU mL^{-1} reduction). More importantly, the dilutions of all 3D materials, except for 3D Gel/EE, of the sponge extracts were also found extremely effective, allowing bacterial growth only at the smallest concentrations (in the following order of performance: 3D PCL/EE, 3D CA/EE, 3D PMMA/EE, Figure 7a). However, to achieve the same effect, 3D Gel/EE extract was required at full concentration. On the contrary, the stock sponge extracts only slightly affected S. aureus cells (Figure 7b). Even after overnight incubation, the gram-positive bacteria grew to the same concentration range as the control. The 2D CA/EE material did not affect any of the bacterial cells at all, as expected. The cationic character of EE is the primary factor contributing to its ability to interact with the negatively charged surfaces of microbial cells.[65,66] However, despite this favorable interaction, 2D CA/EE does not exhibit any bactericidal action. This lack of efficacy can be traced back to the absence of protonated DMAE groups in its structure, which are essential for initiating the antibacterial effect.

The antibacterial effect of 3D samples against *E. coli* can be explained by protonated DMAE groups along the polymer chain, interacting with anionic molecules present on the bacterial surface and destabilizing the bacterial membrane functionality.[67] However, high effectiveness against gram-negative *E. coli*, together with a lack of activity against gram-positive *S. aureus*, is in contradiction to this theory, as phosphate groups on both bacteria are negatively charged.

A selective antibacterial effect against gram-negative bacteria is generally quite exceptional. Structurally, gram-negative bacteria are surrounded by a thin peptidoglycan cell wall surrounded by an outer lipopolysaccharide-based membrane, which is the main reason for their resistance to a wide range of antibiotics, antiseptics or disinfectants[68–70] In fact, these products can even act as their reservoirs, causing the spread of infections.[71] Gram-positive bacteria, in turn, are surrounded by much thicker layers of peptidoglycan but lack an outer membrane and, therefore, are usually easier to eradicate.[69,70]

There are only a few gram-negative specific drugs, including the recently discovered Lolamicin. Gram-negative infections are mostly treated with broad-spectrum antibiotics that disrupt the gut microbiome, leading to secondary infections.[72] Lolamicin interferes with the LolCDE complex that rarely occurs in gram-positive bacteria and disrupts its ability to release outer-membrane-specific lipoproteins from the inner membrane.[73] However, the origin of the gram-negative selectivity of our 3D materials requires a more complex analysis.

The unique combination of structural and functional attributes makes EE an exceptional choice of polymer material,

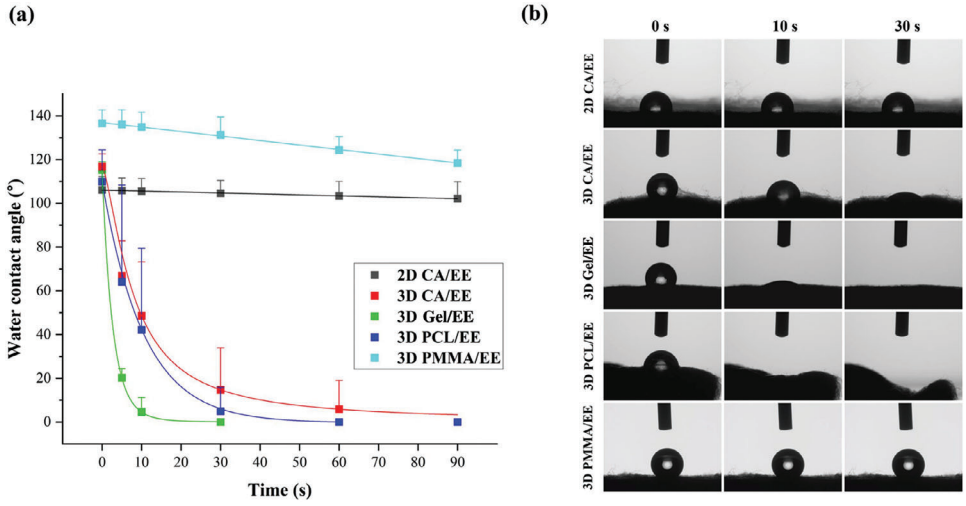

Figure 6. Water contact angles are expressed as mean values with standard deviation versus time of measurement. Data were fitted with linear (2D CA/EE), exponential (3D CA/EE, 3D PCL/EE, and 3D PMMA/EE), and power (3D Gel/EE) curves a). The surface of materials during water contact angle measurements b).

and its protonated form might be used as a substrate for a wide range of applications. Apart from clinical applications, that call for additional material features such as biocompatibility, air filtration is thought to be the most promising. Because of the high porosity accompanied by the lightweight, optimized formulation, the 3D nanofibrous sponges could be utilized in both portable and industrial filters. Data on air-polluting bacteria varies, yet a recent systematic study from urban Spain, considering many environmental factors at different geographical sites, showed a significant predominance of gram-negative bacteria in the air samples.[74] Local environments in Poland, such as pulp and paper mills or sawmills, were found contaminated solely with gram-negative bacteria due to their occurrence in stored timber, posing a risk of respiratory diseases among workers.[75]

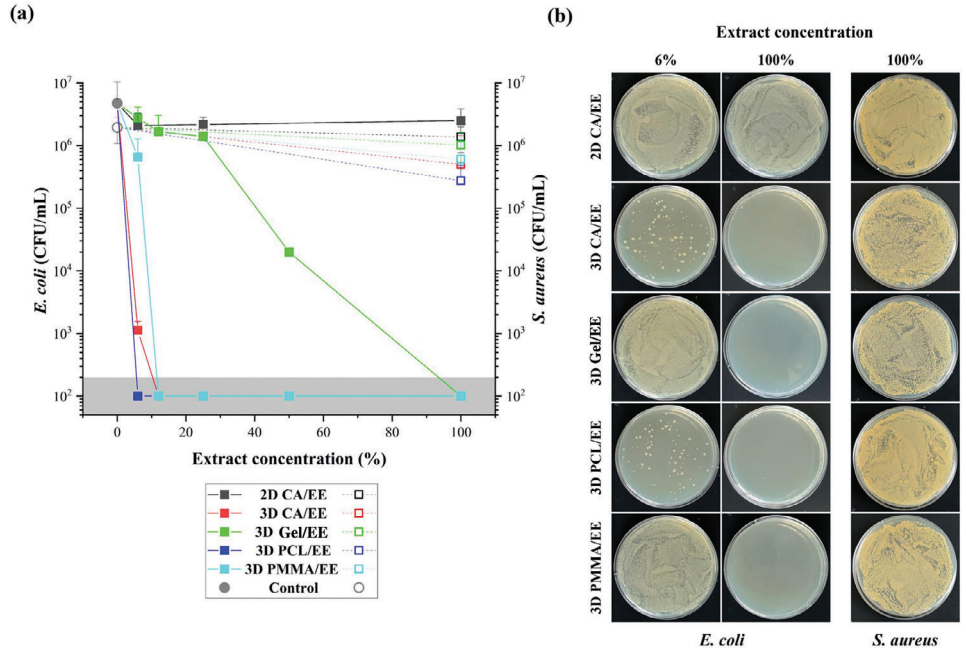

Figure 7. Antibacterial activity of the materials against *E. coli* and *S. aureus*. Colony forming units (CFU) mL^{-1} of *E. coli* and *S. aureus* after 2 h of incubation with material extracts (100% and diluted), expressed as mean values with standard deviation on a logarithmic scale. Filled symbols correspond to *E. coli*, and blank symbols correspond to *S. aureus*. "Control" represents bacterial suspensions of *E. coli* and *S. aureus* allowed for undisturbed growth throughout the incubation period and are plotted at 0% extract concentration. For better visualization, the data points corresponding to one material and control among one species of bacteria are connected with straight lines. Data points below the detection limit (200 CFU mL^{-1}, filled down with gray color) are set to 50 CFU mL^{-1} a). Photo set of agar plates presenting bacterial growth of *E. coli* and *S. aureus* after contact with material extracts b).

4. Conclusion

In this study, 3D nanofibrous sponges were successfully fabricated by utilizing conventional electrospinning of polymer blends without the necessity of additional steps or equipment. The presence of protonated dimethylaminoethyl (DMAE) groups in Eudragit E100 played a key role in the structure formation and possessed unique collective properties. The in situ protonated DMAE groups, confirmed by several methods and techniques, were responsible for creating a fluffy nanofibrous macrostructure through electrostatic repulsion and gave the resulting nanofibers strong antibacterial properties against gram-negative bacteria like *E. coli*, selectively. This unique combination of structural and functional attributes makes the generated electrospun nanofibers an exceptional choice of nanostructured functional material for a wide range of applications. The 3D nanofibrous sponge might be used to complement traditional filtering membranes, especially in filtration cartridges used for personnel masks. Furthermore, they can be an option for integration into filtering sheets in large-scale HVAC (heating, ventilation, and air conditioning) systems to increase antibacterial efficiency. Additionally, the strategy to fabricate 3D nanofibrous sponges can be utilized as a platform to integrate a wide array of functional materials into 3D structures, enhancing their effectiveness through an increased surface area and with the availability of interaction sites.

Supporting Information

Supporting Information is available from the Wiley Online Library or from the author.

Acknowledgements

Author AA sincerely acknowledges the financial support from the Alexander von Humboldt Foundation (Experienced Researcher Fellowship, grant agreement ID: MNG 1237848 HFST-E) and ERA.Net RUS Plus funding mechanism (Project Bioresorbable implantable triboelectric nanogenerator devices, "BIOTENG-01DJ21011"). We acknowledge support by the Open Access Publication Fund of Rhine-Waal University of Applied Sciences.

Conflict of Interest

The authors declare no conflict of interest.

Data Availability Statement

The data that support the findings of this study are available from the corresponding author upon reasonable request.

Keywords

3D nanofibrous sponges, antibacterial activity, electrospinning, in situ protonation, polymer blends

Received: November 22, 2024
Revised: January 31, 2025
Published online:

[1] A. Sionkowska, *Prog. Polym. Sci.* **2011**, *36*, 1254.
[2] A. Amarjargal, M. Brunelli, G. Fortunato, F. Spano, C. S. Kim, R. M. Rossi, *J. Drug. Delivery. Sci. Technol.* **2019**, *52*, 8.
[3] R. Schneider, M. H. M. Facure, P. A. M. Chagas, R. S. Andre, D. M. dos Santos, D. S. Correa, *Adv. Mater. Interfaces.* **2021**, *8*, 2100430.
[4] H. Zhong, J. Huang, J. Wu, J. Du, *Nano Res.* **2021**, *15*, 787.
[5] A. Amarjargal, O. Cegielska, D. Kolbuk, B. Kalaska, P. Sajkiewicz, *ACS Appl. Mater. Interfaces.* **2024**, *16*, 153.
[6] L. E. Aguilar, A. R. Unnithan, A. Amarjargal, A. P. Tiwari, S. T. Hong, C. H. Park, C. S. Kim, *Int. J. Pharm.* **2015**, *478*, 1.
[7] V. P. Nirwan, A. Amarjargal, R. Hengsbach, A. Fahmi, *Macromol. Rapid Commun.* **2024**, 2400617.
[8] P. Arora, Z. Zhang, *Chem. Rev.* **2004**, *104*, 4419.
[9] X. Song, Z. Wang, F. Zhao, Y. Sun, B. Cheng, J. Xing, *Adv. Mater. Interfaces.* **2021**, *8*, 2100458.
[10] H. Lee, M. Yanilmaz, O. Toprakci, K. Fu, X. Zhang, *Energy Environ. Sci.* **2014**, *7*, 3857.
[11] L. Cao, Y. Si, X. Yin, J. Yu, B. Ding, *ACS Appl. Mater. Interfaces* **2019**, *11*, 35333.
[12] G. Liang, W. Zhang, X. Zhang, J. Yu, S. Zhang, B. Ding, *Comp. Commun.* **2024**, *50*, 102006.
[13] F. Deuber, S. Mousavi, L. Federer, M. Hofer, C. Adlhart, *ACS Appl. Mater. Interfaces.* **2018**, *10*, 9069.
[14] Y. Si, J. Yu, X. Tang, J. Ge, B. Ding, *Nat. Commun.* **2014**, *5*, 5802.
[15] S. Dong, B. Maciejewska, R. Millar, N. Grobert, *Adv. Compos. Hybrid Mater.* **2023**, *6*, 1.
[16] P. Risch, C. Adlhart, *Chimia (Aarau)* **2022**, *76*, 354.
[17] N. S. Sharma, A. Karan, H. Q. Tran, J. V. John, S. M. Andrabi, S. M. Shatil Shahriar, J. Xie, *Acta Biomater.* **2024**, *184*, 81.
[18] G. Cheng, J. Dai, J. Dai, H. Wang, S. Chen, Y. liu, X. Liu, X. Li, X. Zhou, H. Deng, Z. Li, *Chem. Eng. J.* **2021**, *410*, 128379.
[19] A. R. Unnithan, A. R. K. Sasikala, S. S. Thomas, A. G. Nejad, Y. S. Cha, C. H. Park, C. S. Kim, *Sci. Rep.* **2018**, *8*, 5696.
[20] Y. Chen, X. Dong, M. Shafiq, G. Myles, N. Radacsi, X. Mo, *Adv. Fiber. Mater.* **2022**, *4*, 959.
[21] Y. Song, S. Zhao, K. Li, Z. Fei, G. Chen, Z. Yang, *Prog. Chem.* **2023**, *35*, 11.
[22] L. Bao, Z. Zhang, X. Li, L. Zhang, H. Tian, M. Zhao, T. Ye, W. Cui, *Small* **2023**, *19*, 2303615.
[23] X. Fu, J. Wang, D. Qian, L. Xi, L. Chen, Y. Du, W. Cui, Y. Wang, *Adv. Fiber. Mater.* **2023**, *5*, 1773.
[24] X. Fu, J. Wang, D. Qian, Z. Chen, L. Chen, W. Cui, Y. Wang, *Adv. Fiber. Mater.* **2023**, *5*, 979.
[25] A. Amarjargal, Z. M. Goudarzi, O. Cegielska, A. Gradys, D. Kolbuk, B. Kalaska, A. Ruszczyńska, P. Sajkiewicz, *Cite this: Biomater. Sci.* **2023**, *11*, 5502.
[26] G. Duan, M. Koehn-Serrano, A. Greiner, *Macromol. Rapid Commun.* **2017**, *38*, 1600511.
[27] F. Deuber, S. Mousavi, L. Federer, C. Adlhart, *Adv. Mater. Interfaces.* **2017**, *4*, 1700065.
[28] J. Jiang, S. Chen, H. Wang, M. A. Carlson, A. F. Gombart, J. Xie, *Acta Biomater.* **2018**, *68*, 237.
[29] X. Xie, D. Li, Y. Chen, Y. Shen, F. Yu, W. Wang, Z. Yuan, Y. Morsi, J. Wu, X. Mo, *Adv. Healthcare Mater.* **2021**, *10*, 2100918.
[30] J. I. Kim, J. C. Lee, M. J. Kim, C. H. Park, C. S. Kim, *Mater. Lett.* **2019**, *236*, 510.
[31] X. Cheng, Y. T. Liu, Y. Si, J. Yu, B. Ding, *Nat. Commun.* **2022**, *13*, 1.
[32] H. Y. Mi, X. Jing, H. X. Huang, L. S. Turng, *Mater. Lett.* **2017**, *204*, 45.
[33] S. H. Cho, S. Lee, J. I. Kim, *Sci. Rep.* **2024**, *14*, 1.
[34] J. Y. Kim, J. I. Kim, C. H. Park, C. S. Kim, *Mater. Lett.* **2019**, *236*, 521.
[35] A. Chinnakorn, Y. Soi-Ngoen, O. Weeranantanapan, P. Pakawanit, S. Maensiri, K. Srisom, P. Janphuang, N. Radacsi, W. Nuansing, *ACS Biomater. Sci. Eng.* **2024**, *10*, 5336.

[36] S. Lee, M. K. Joshi, A. P. Tiwari, B. Maharjan, K. S. Kim, Y. H. Yun, C. H. Park, C. S. Kim, *Chem. Eng. J.* **2018**, *347*, 771.
[37] S. Cai, H. Xu, Q. Jiang, Y. Yang, *Langmuir* **2013**, *29*, 2311.
[38] S. Dong, B. M. Maciejewska, M. Lißner, D. Thomson, D. Townsend, R. Millar, N. Petrinic, N. Grobert, *ACS Nano* **2023**, *17*, 6810.
[39] R. Li, X. Deng, F. Liu, Y. Yang, Y. Zhang, N. Reddy, W. Liu, Y. Qiu, Q. Jiang, *Nanoscale* **2020**, *12*, 16690.
[40] S. Thakral, N. K. Thakral, D. K. Majumdar, *Expert. Opin. Drug. Delivery.* **2013**, *10*, 131.
[41] C. A. Bonino, S. I. Jeong, M. D. Krebs, E. Alsberg, S. A. Khan, *Small* **2012**, *8*, 1928.
[42] H. Okuzaki, T. Takahashi, N. Miyajima, Y. Suzuki, T. Kuwabara, *Macromolecules* **2006**, *39*, 4276.
[43] V. Linares, C. J. Yarce, J. D. Echeverri, E. Galeano, C. H. Salamanca, *Polymers* **2019**, *11*, 1010.
[44] S. Shikha, Y. W. Lee, P. S. Doyle, S. A. Khan, *Mol Pharm.* **2022**, *19*, 4345.
[45] J. J. Carrascal, R. Pinal, T. Carvajal, L. D. Pérez, Y. Baena, *Int. J. Pharm.* **2021**, *607*, 120991.
[46] Y. M. Pupo, P. V. Farago, J. M. Nadal, L. A. Esmerino, D. F. Maluf, S. F. Zawadzki, M. D. Michél, F. A. Dos Santos, O. M. M. Gomes, J. C. Gomes, *J. Biomater. Sci. Polym. Ed.* **2013**, *24*, 1443.
[47] F. Leal, V. Nirwan, A. M. Gonçalves, N. Panitschewski, E. Filová, A. Fahmi, P. F. Costa, *Int. J. Polym. Mater. Polym. Biomater.* **2024**, *73*, 1054.
[48] L. Deng, X. Zhang, Y. Li, F. Que, X. Kang, Y. Liu, F. Feng, H. Zhang, *Food Hydrocoll.* **2018**, *75*, 72.
[49] J. H. Ko, H. Yin, J. An, D. J. Chung, J. H. Kim, S. B. Lee, D. G. Pyun, *Macromol. Res.* **2010**, *18*, 137.
[50] T. Parikh, S. S. Gupta, A. K. Meena, A. T. Serajuddin, *J. Excipients Food Chem.* **2014**, *5*, 54.
[51] J. Lee, J. Y. Moon, J. C. Lee, T. I. Hwang, C. H. Park, C. S. Kim, *Carbohydr. Polym.* **2021**, *253*, 117191.
[52] V. P. Nirwan, E. Filova, A. Al-Kattan, A. V. Kabashin, A. Fahmi, *Nanomaterials* **2021**, *11*, 519.
[53] L. S. Chen, Z. M. Huang, G. H. Dong, C. L. He, L. Liu, Y. Y. Hu, Y. Li, *Polym. Compos.* **2009**, *30*, 239.
[54] S. Eisold, L. H. Alvarez, K. Ran, R. Hengsbach, G. Fink, S. Centeno Benigno, J. Mayer, D. Wöll, U. Simon, *Nanoscale* **2021**, *13*, 2875.
[55] U. Böhme, U. Scheler, *Macromol. Chem. Phys.* **2007**, *208*, 2254.
[56] R. Hengsbach, G. Fink, U. Simon, *Soft Matter* **2024**, *20*, 330.
[57] G. Kocak, C. Tuncer, V. Bütün, *Polym. Chem.* **2016**, *8*, 144.
[58] S. de Ávila Gonçalves, J. H. L. da Fonsêca, M. A. d'Ávila, R. P. Vieira, *Int. J. Biol. Macromol.* **2024**, *277*, 134168.
[59] F. Mikaeili, P. I. Gouma, *Sci. Rep.* **2018**, *8*, 1.
[60] I. Elaissaoui, S. Sayeb, I. Ounif, M. Ferhi, H. naifer Karima, D. J. Ennigrou, *Heliyon* **2024**, *10*, e32552.
[61] J. Dulnik, P. Denis, P. Sajkiewicz, D. Kołbuk, E. Choińska, *Polym. Degrad. Stab.* **2016**, *130*, 10.
[62] S. Sivakumar, R. Schmid, A. Wieland, P. L. Strissel, R. Strick, L. Fischer, I. Thievessen, E. Kataev, A. Arkudas, R. E. Horch, D. W. Schubert, A. Kengelbach-Weigand, *Adv. Mater. Interfaces.* **2022**, *9*, 2101808.
[63] J. A. Nychka, M. M. Gentleman, *JOM* **2010**, *62*, 39.
[64] M. Li, X. Liu, N. Liu, Z. Guo, P. K. Singh, S. Fu, *Colloids Surf A Physicochem Eng Asp.* **2018**, *554*, 122.
[65] V. L. Romero, P. Pons, J. L. Bocco, R. H. Manzo, F. L. Alovero, F. Alovero, *FEMS Microbiol. Lett.* **2012**, *334*, 102.
[66] M. B. Corti, L. P. Campagno, V. L. Romero, S. Gutierrez, F. L. Alovero, *Arch. Microbiol.* **2022**, *204*, 507.
[67] A. M. Carmona-Ribeiro, L. D. de Melo Carrasco, *Int. J. Mol. Sci.* **2013**, *14*, 9906.
[68] D. Saxena, R. Maitra, R. Bormon, M. Czekanska, J. Meiers, A. Titz, S. Verma, S. Chopra, *npj Antimicrobials. Resistance.* **2023**, *1*, 17.
[69] R. M. Epand, R. F. Epand, *Biochimica et Biophysica Acta (BBA) – Biomembranes.* **2009**, *1788*, 289.
[70] Z. Breijyeh, B. Jubeh, R. Karaman, *Molecules* **2020**, *25*, 1340.
[71] P. Lompo, A. S. Heroes, E. Agbobli, A. Kazienga, M. Peeters, H. Tinto, K. Lagrou, L. Sangaré, D. Affolabi, J. Jacobs, *Pathogens* **2023**, *12*, 917.
[72] H. I. Zgurskaya, V. V. Rybenkov, *Ann. N. Y. Acad. Sci.* **2020**, *1459*, 5.
[73] K. A. Muñoz, R. J. Ulrich, A. K. Vasan, M. Sinclair, P. C. Wen, J. R. Holmes, H. Y. Lee, C. C. Hung, C. J. Fields, E. Tajkhorshid, G. W. Lau, P. J. Hergenrother, *Nature* **2024**, *630*, 429.
[74] D. Rojo, M. A. Rojo, T. Girbes, D. Rojo, M. A. Rojo, T. Girbes, *Open. J. Air. Pollution.* **2021**, *10*, 31.
[75] A. Wójcik-Fatla, B. Mackiewicz, A. Sawczyn-Domańska, J. Sroka, J. Siwiec, M. Paściak, B. Szponar, K. Pawlik, J. Dutkiewicz, *Int. Arch. Occup. Environ. Health.* **2022**, *95*, 1179.